Chemistry
A European Journal

Chemistry
Europe
European Chemical
Societies Publishing

Accepted Article

Title: Origin of Stereoselectivity in SE2' Reactions of Six-membered Ring Oxocarbenium Ions

Authors: Wouter A. Remmerswaal, Thomas Hansen, Trevor Hamlin, and Jeroen D. C. Codée

To be cited as: *Chem. Eur. J.* **2022**, e202203490

Link to VoR: https://doi.org/10.1002/chem.202203490

WILEY-VCH

Origin of Stereoselectivity in S_E2' Reactions of Six-membered Ring Oxocarbenium Ions

Wouter A. Remmerswaal,[a] Thomas Hansen,*[a,b] Trevor A. Hamlin,*[b] Jeroen D. C. Codée*[a]

[a] Wouter A. Remmerswaal, Dr. Thomas Hansen, Prof. Dr. Jeroen D. C. Codée. Leiden Institute of Chemistry, Leiden University, Einsteinweg 55, 2333 CC Leiden, The Netherlands. Email: t.hansen@vu.nl, jcodee@chem.leidenuniv.nl.

[b] Dr. Thomas Hansen, Dr. Trevor A. Hamlin. Department of Theoretical Chemistry, Amsterdam Institute of Molecular and Life Sciences (AIMMS), Amsterdam Center for Multiscale Modeling (ACMM), Vrije Universiteit Amsterdam, De Boelelaan 1083, 1081 HV Amsterdam, The Netherlands. Email: t.a.hamlin@vu.nl.

Abstract

Oxocarbenium ions are key reactive intermediates in organic chemistry. To generate a series of structure−reactivity-stereoselectivity principles for these species, we herein investigated the bimolecular electrophilic substitution reactions (S_E2') between allyltrimethylsilane and a series of archetypal six-membered ring oxocarbenium ions using a combined density functional theory (DFT) and coupled-cluster theory approach. These reactions preferentially proceed following a reaction path where the oxocarbenium ion transforms from a half chair ($^3H_4$ or $^4H_3$) to a chair conformation. The introduction of alkoxy substituents on six-membered ring oxocarbenium ions, dramatically influences the conformational preference of the canonical $^3H_4$ and $^4H_3$ conformers, and thereby the stereochemical outcome of the S_E2' reaction. In general, we find that the stereoselectivity in the reactions correlates to the "intrinsic preference" of the cations, as dictated by their shape. However, for the C5-CH_2OMe substituent, steric factors override the "intrinsic preference", showing a more selective reaction than expected based on the shape of the ion. Our S_E2' energetics correlate well with experimentally observed stereoselectivity, and the use of the activation strain model has enabled us to quantify important interactions and structural features that occur in the transition state of the reactions to precisely understand the relative energy barriers of the diastereotopic addition reactions. The fundamental mechanistic insight provided in this study will aid in understanding the reactivity of more complex glycosyl cations featuring multiple substituents and will facilitate our general understanding of glycosylation reactions.

Keywords: Activation strain model; Bimolecular electrophilic substitutions; Density functional theory calculations; Oxocarbenium Ions; Reactivity.

Introduction

Six-membered ring oxocarbenium ions are important reactive intermediates in bioorganic and synthetic organic chemistry.[1] Carbohydrate processing enzymes, such as glycosyltransferases and hydrolases, transfer or cleave carbohydrates to or from their substrates. These reactions proceed through transition states, in which a significant amount of oxocarbenium character builds up in the carbohydrate moiety that is transferred or cleaved.[2] In synthetic carbohydrate chemistry, the stability of oxocarbenium ions determines the reactivity of glycoside donor building blocks and plays a central role in the stereochemical outcome of glycosylation reaction.[3] Despite the high reactivity of these species, they can react with excellent stereoselectivity, and it has been shown that many glycosyl oxocarbenium ions can provide reaction products with striking 1,2-*cis* selectivity.[4] The fleeting nature of oxocarbenium ions represents a major challenge in studying these species and determining clear structure-reactivity-stereoselectivity principles. Recently, direct spectroscopic evidence for glycosyl oxocarbenium ions has been provided in the gas-phase using state-of-the-art IR spectroscopy and in super acid media (to guarantee a sufficient lifetime of the species) using NMR spectroscopy.[5] DFT calculations have provided detailed insight into the stereoelectronic effects of the substituents on the structure, stability and reactivity of these ions.[4,6]

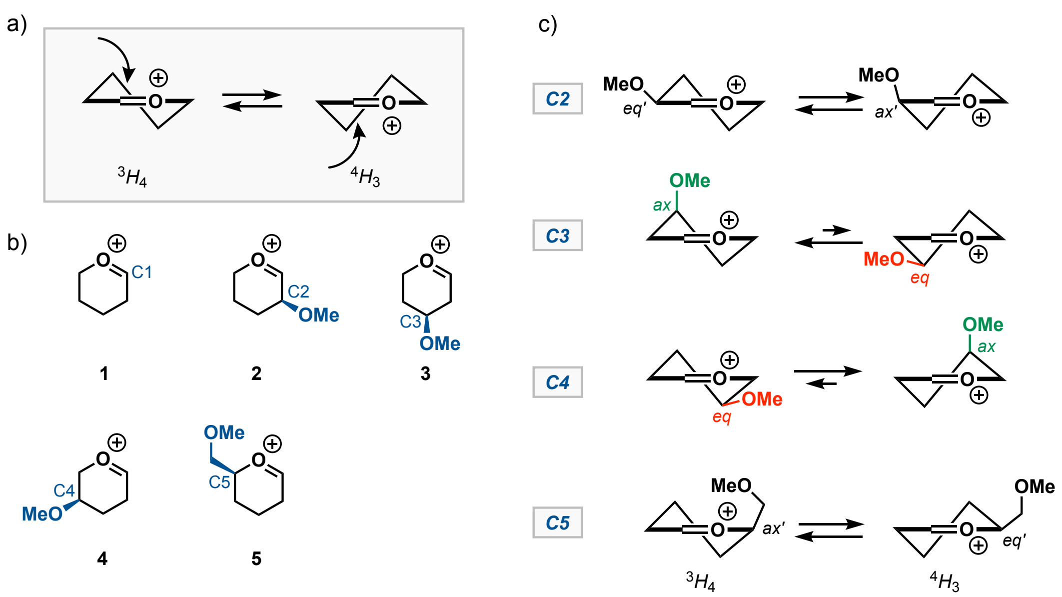

Scheme 1. (a) The conformational equilibrium between the $^3H_4$ and $^4H_3$ with the face preference following a chair-like TS; (b) Computationally analyzed substituted oxocarbenium ions, *i.e.*, cation **1**-**5**; (c) Conformational preference (green = stabilizing; red = destabilizing) of mono-substituted six-membered oxocarbenium ions reflected by the isolated product ratios (*i.e.*, diastereoselectivity) from the seminal work of Woerpel *et al*,[7] in which ax(') = (*pseudo*-)axial and eq(') = (*pseudo*-)equatorial.

Generally, oxocarbenium ions adopt a flattened structure, as a consequence of the stabilization of the electron-depleted cationic carbon by the adjacent electron-rich ring-oxygen, adopting a $^{3}H_{4}$ or $^{4}H_{3}$ conformation (Scheme 1a).[8] It has been proposed that these half chair conformers are preferentially attacked at the diastereotopic face that leads to a low energy chair-like transition state as opposed to the other face, which provides a twist boat-like transition state (Scheme 2).[9] Consequently, the $^{3}H_{4}$ will form a top-face product (Scheme 1a), while a bottom-face product is found for the opposite $^{4}H_{3}$ half chair. It is known that substituents on the ring can dramatically affect the conformational preference of the six-membered cation, and thus the stereochemical outcome of reactions with these cations.[10] Substituted cyclic oxocarbenium ions with electron-rich substituents (*e.g.*, *O*-, *N*-, *F*-groups) at the C3- and C4-position of the ring prefer to adopt an axial position, presumably to stabilize the cationic center by electrostatic and orbital interactions (Scheme 1b and 1c).[7] When these groups are present on the C2-position, they have a very slight preference to adopt a *pseudo*-equatorial position, enabling hyperconjugative stabilization by the *pseudo*-axial $\sigma_{C2\text{–}H2}$ bond of the oxocarbenium ion. Despite spectroscopic and computational studies that have provided a detailed understanding of the conformational behavior of six-membered oxocarbenium ions,[4] quantitative insight into the factors controlling the reactions taking place on these ions is largely lacking.

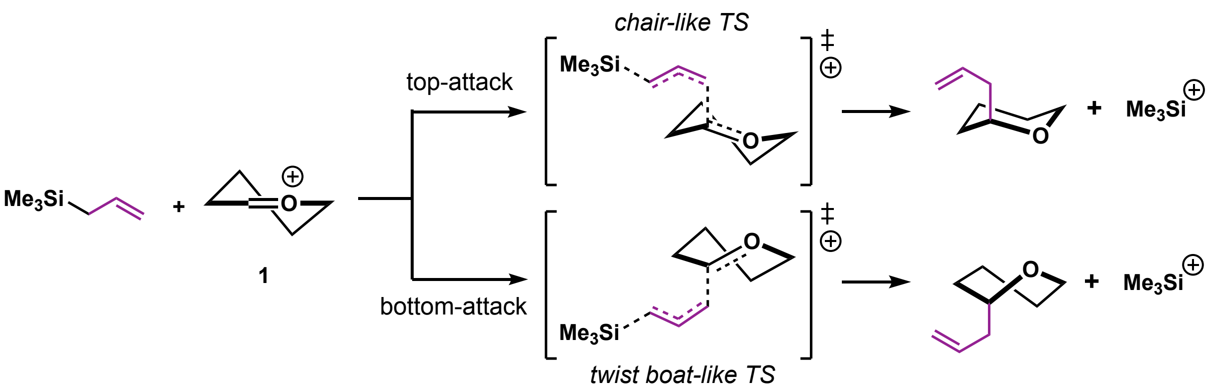

Scheme 2. Top face-attack (*i.e.*, chair-like TS) and bottom face-attack (*i.e.*, twist boat-like TS) of the S_E2' reaction between allyltrimethylsilane and $^{3}H_{4}$ oxocarbenium ion **1**. The reaction follows a transfer reaction by a bimolecular electrophilic substitution mechanism (S_E2'), in which an allylic-group (purple) is transferred between two electrophilic moieties.[11]

To study how stereoelectronic effects impact the stereoselectivity of six-membered oxocarbenium ions, we computationally explored the reaction profile of reactions between allyltrimethylsilane and a series of oxocarbenium ions **1-5** using density functional theory at PCM(CH_2Cl_2)-B3LYP/6-311G(d,p) (Scheme 1b and Scheme 2). We have also computed high accuracy DLPNO-CCSD(T)[12] reference data, confirming the reliability of our DFT method.

 10.1002/chem.202203490

We selected allyltrimethylsilane as a typical *C*-nucleophile that requires a strong electrophile, such as an oxocarbenium ion intermediate, to react.[4] These reactions follow a bimolecular electrophilic substitution reaction path (S_E2'), in which an allylic-group (purple in Scheme 2) is transferred to the electrophilic oxocarbenium ion by the expulsion of the electrophilic Me_3Si^+ leaving-group.[13] The analyzed oxocarbenium ions **2-5** have a single ring substituent on the six-membered ring at the C2-, C3-, C4-, or C5-position (see Scheme 1b), to map the effects of these substituents as a function of their position in the ring. To furnish quantitative insight into the electronic factors governing in these S_E2' reactions, we employed the activation strain model (ASM)[14] and Kohn-Sham molecular orbitals (KS-MO).[15]

Results and Discussion

Structure and Reactivity Trends

The results of the computed reaction profiles and structural data of the S_E2' reaction between allyltrimethylsilane and cations **1-5** are summarized in Figure 1 – 3 (for interested readers, all the data on the stationary points can be found in the SI Table S1, S2 and S3). Note that all reactivity trends are consistent for ΔG and ΔE (Table S1). Importantly, the computed trends in reactivity at PCM(CH_2Cl_2)-B3LYP/6-311G(d,p) agree well with computed energies at the more accurate SMD(CH_2Cl_2)-(TightPNO)DLPNO-CCSD(T)/CBS(3,4/def2) level (Table S1 and S2).[16] Figure 1 shows the structures of the two possible transition states following a chair-like or twist boat-like TS of cation **1**, in which both electrophilic species, *i.e.*, trimethylsilyl leaving group and oxocarbenium ion, are orientated in an antiperiplanar fashion, both interacting with

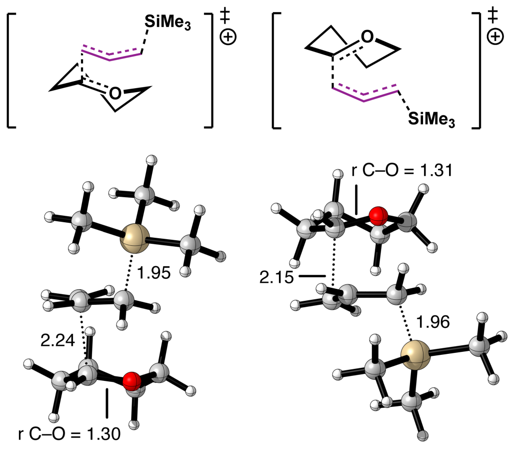

Figure 1. Transition state structures with key bond lengths (in Å) for the S_E2' reactions between allyltrimethylsilane and oxocarbenium ion **1** following a top face-attack, *i.e.*, chair-like TS, and bottom face-attack, *i.e.*, twist boat-like TS, computed at PCM(CH_2Cl_2)-B3LYP/6-311G(d,p).

the allyl moiety (highlighted in purple in Figure 1). As anticipated, we found for cation **1** that the chair-like TS is more than 4 kcal mol^{-1} lower in energy than the reaction barrier of the twist boat-like TS using DFT computations (Table S1 and S2 for all reaction profile data).

For the unsubstituted oxocarbenium ion **1**, the $^{3}H_{4}$ and $^{4}H_{3}$ structures are chemically equivalent, but introducing a substituent on the six-membered ring gives rise to two chemically different structures. We found that these two reactants, $^{3}H_{4}$-R and $^{4}H_{3}$-R, are in rapid equilibrium with each other by a relatively low interconversion barrier via the $B_{2,5}$ or $^{2,5}B$ conformer, setting the stage for a Curtin-Hammett scenario (Figure 2 and 3).[17] In this case, the reaction barrier difference, $\Delta\Delta G^{‡}$, dictates the product distribution. If (i) $\Delta G^{o}{}_{3H4}$ is lower in energy than $\Delta G^{o}{}_{4H3}$, as for cation **2** and **3**, $\Delta\Delta G^{‡} = (\Delta G^{‡}{}_{4H3\text{-bottom}} + \Delta G^{o}{}_{4H3}) - \Delta G^{‡}{}_{3H4\text{-top}}$, while if (ii) $\Delta G^{o}{}_{3H4}$ is higher in energy than $\Delta G^{o}{}_{4H3}$, as for cation **4** and **5**, $\Delta\Delta G^{‡} = \Delta G^{‡}{}_{4H3\text{-bottom}} - (\Delta G^{‡}{}_{3H4\text{-top}} + \Delta G^{o}{}_{3H4})$.[18]

Several distinct trends emerge from the computed reaction profiles for cations **2-5** (Figure 2 and 3). Firstly, in line with cation **1**, cation **2-5** all favor the chair-like TS over the twist boat-like TS ($\Delta\Delta G^{‡}{}_{\text{twist boat-chair}} = \sim +3\text{–}5$ kcal mol^{-1}). This reinforces the notion that the half chair conformers exclusively react via the chair-like TS for these model systems. Secondly, the lowest overall reaction barrier found for the different cations decreases from +12.4, +12.1, +10.9, +8.4 kcal mol^{-1} for cations **5**, **4**, **3**, **2**, placing the alkoxy substituent gradually closer in space (respectively 4.10, 3.32, 3.11 and 2.37 Å in the equilibrium geometry) to the electrophilic C1-position. The lower reaction barrier is a direct effect of the electron-withdrawing character of the substituent, which stepwise increases the electron-accepting capability of the C1-cation. For all systems, there is a parallel between the $\Delta\Delta G^{‡}$ of the overall reactions and the lowest energy oxocarbenium ion conformer (highlighted in purple in Figure 2 and 3). These findings are in line with our previous work, in which we could relate the stereoselectivity in addition reactions of allyltrimethylsilane and triethylsilane to the conformational preference of pyranosyl and furanosyl oxocarbenium ions.[4] Cation **3** (3-OMe) favors the $^{3}H_{4}$ conformation, which is attacked from the top face, resulting in a *cis*-product (Figure 3b). In contrast, cations **4** and **5** prefer the opposite $^{4}H_{3}$ half chair, which preferentially reacts on the bottom face (Figure 2d and 3b), delivering the *trans*-product. Note, that cation **5** only has a very slight preference for the $^{4}H_{3}$. Cation **2** has no clear preference for either half chairs, which results in a mixture of *cis*- and *trans*-products (Figure 3d). Overall, the computed stereoselectivity, derived from the $\Delta\Delta G^{‡}$ values, correlates well with the available experimental result by Woerpel and co-workers.[4a,7]

10.1002/chem.202203490

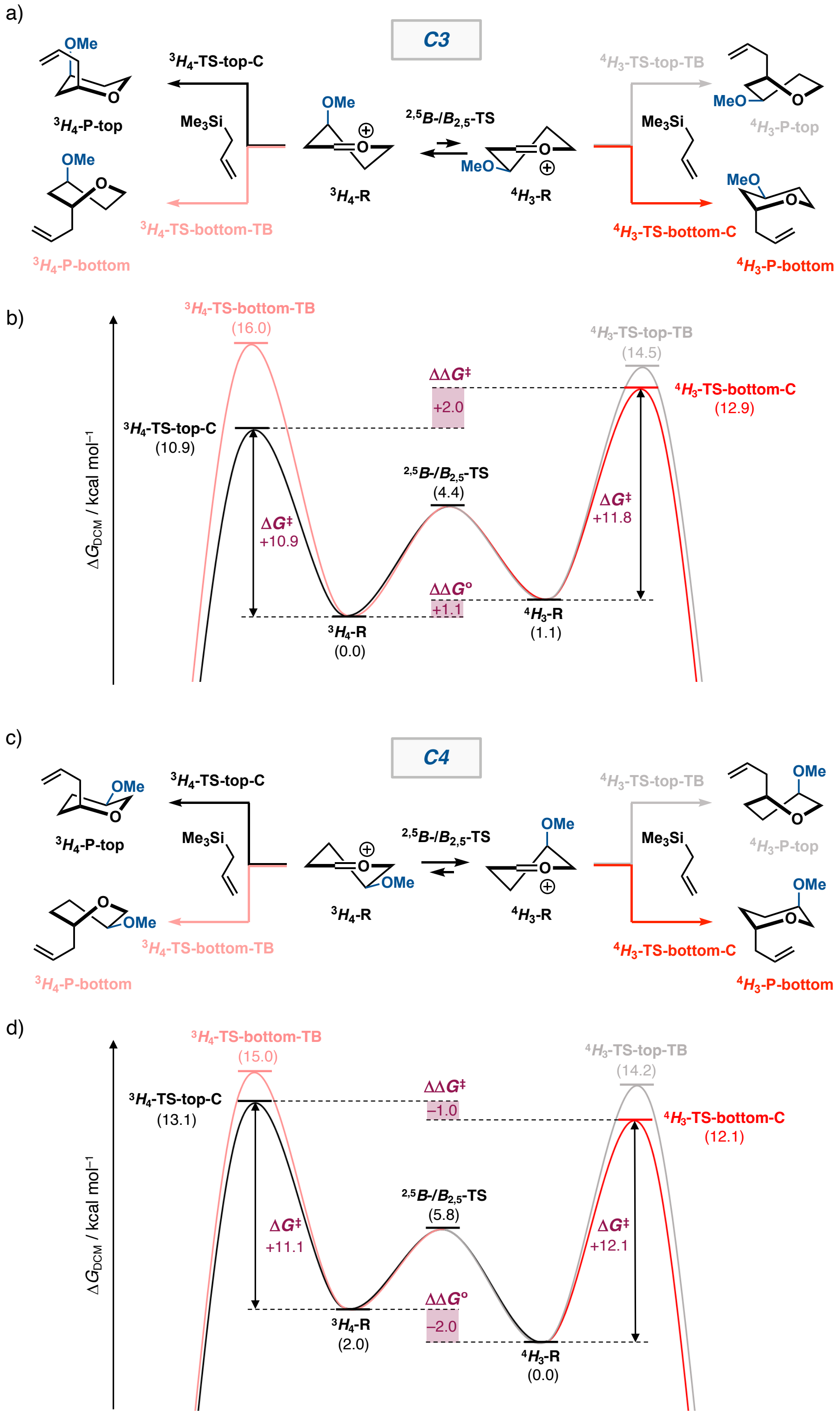

Figure 2. The possible S_E2' reaction pathways and the corresponding reaction profile of cation **3** (a,b) and **4** (c,d) of the top- (black: chair-like TS path, grey; twist boat-like TS path) and bottom attack (red: chair-like TS path; pink: twist boat-like TS path) at the $^3H_4$ and $^4H_3$ conformations. Gibbs energies in dichloromethane (ΔG_{DCM}, in kcal mol^{-1}) relative to reactants. See SI Table S1 for all data of the stationary points of the reaction profiles, including the products.

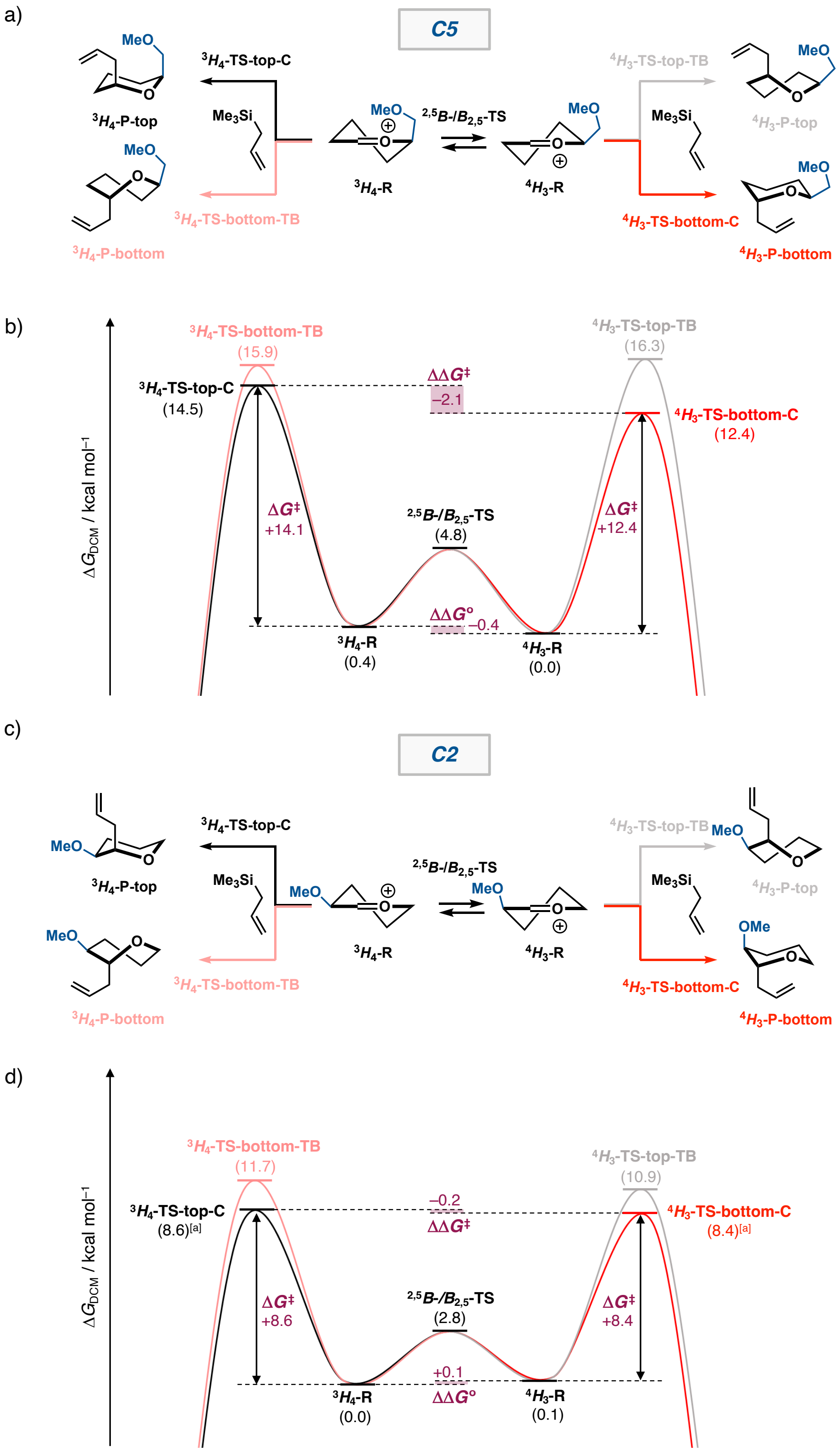

Figure 3. The possible S_E2' reaction pathways and the corresponding reaction profile of cation **5** (a,b) and **2** (c,d) of the (black: chair-like TS path; grey: twist boat-like TS path) and bottom attack (red: chair-like TS path; pink: twist boat-like TS path) at the $^{3}H_{4}$ and $^{4}H_{3}$ conformations. Gibbs energies in dichloromethane (ΔG_{DCM}, in kcal mol^{-1}) relative to reactants. See SI Table S1 for all data of the stationary points of the reaction profiles, including the products. [a] Reaction barriers could not be located on the electronic energy surface, and an accurate approximation of the barrier was made based on the Gibbs energy surface (see methods section in the SI for details).

Importantly, differences are observed between the conformational preference of the cation ($\Delta\Delta G^{o}$) and the relative differences of the overall barriers ($\Delta\Delta G^{\ddagger}$), which we will explain in detail. For example, Figure 3b shows that cation **5** has a very small preference for the $^{4}H_{3}$ conformation over the $^{3}H_{4}$ ($\Delta\Delta G^{o}$ = –0.4 kcal mol^{-1} for the $^{4}H_{3}$ relative to the $^{3}H_{4}$), but the relative overall reaction barriers for the two $^{1}C_{4}$ and $^{4}C_{1}$ chair like-like TSs, originating from respectively the $^{3}H_{4}$ or the $^{4}H_{3}$ conformer, show a larger difference ($\Delta\Delta G^{\ddagger}$ = –2.1 kcal mol^{-1}). This leads to a more *trans*-selective reaction than what would be expected based on the intrinsic conformational preference of the cation.

The difference in energy of the two conformers of cation **4** (Figure 2d, $\Delta\Delta G^{o}$ = –2.0 kcal mol^{-1} for the $^{4}H_{3}$ relative to the $^{3}H_{4}$) is partly diminished in the transition states of the $S_{E}2'$ reactions originating from these ($\Delta\Delta G^{\ddagger}$ = –1.0 kcal mol^{-1}). For cation **3** (Figure 2b), we found that the difference in the reaction barriers ($\Delta\Delta G^{\ddagger}$ = +2.0 kcal mol^{-1} for the $^{4}H_{3}$ relative to the $^{3}H_{4}$) is significantly larger than the conformational preference of the cation ($\Delta\Delta G^{o}$ = +1.1 kcal mol^{-1}). For cation **2** (Figure 3d), there is no clear preference between both half chair conformers ($\Delta\Delta G^{o}$ = +0.1 kcal mol^{-1} for the $^{4}H_{3}$ relative to the $^{3}H_{4}$), and also the corresponding transition states show only a marginal difference ($\Delta\Delta G^{\ddagger}$ = –0.2 kcal mol^{-1} for the $^{4}H_{3}$ relative to the $^{3}H_{4}$).

Activation strain analyses

To gain quantitative insight into the physical factors controlling the facial selectivity of the additions to either face of the half chair conformations (*i.e.*, the chair-like TS versus the twist boat-like TS), we turned to the activation strain model (ASM) of reactivity.[14] The ASM is a fragment-based approach in which the reaction profile can be described with respect to, and understood in terms of, the characteristics of the reactants, *i.e.*, allyltrimethylsilane and the oxocarbenium ion (see method section for more details). The ASM decomposes the total energy (ΔE) into strain energy (ΔE_{strain}) and interaction energy (ΔE_{int}). In the herein presented activation strain diagrams (ASDs), the intrinsic reaction coordinate (IRC) is projected onto the carbon–leaving group (C•••Si) stretch. This critical reaction coordinate undergoes a well-defined change during the reaction from the reactants via the transition state to the product and is shown to be a valid reaction coordinate for studying bimolecular reactions.

Figure 4a shows that the top face-attack (black line) at the unsubstituted oxocarbenium ion **1** via a chair-like TS proceeds with a significantly lower barrier than the bottom face-attack (pink line) via a twist boat-like TS (see Figure S1, S2 and S3 for ASM data of the full reaction profile for all studied systems, both in solution and gas-phase). Figure 4 reveals that this facial selectivity originates from a more stabilizing interaction energy, which develops in the reaction pathway via the chair-like TS, while the strain curves are very similar for both faces of attack. The more stabilizing interaction energy is a direct effect of the more efficient deformation of the half chair to chair-like TS, as it does not lead to eclipsing interactions between the C1–H and the *pseudo*-equatorial C2–H, in contrast to the twist boat-like TS (Figure 4b). The more efficient deformation allows the chair-like TS to have a larger degree of the pyramidalization of the C1-position, *i.e.*, C2–(H)C1=O$^+$, than the twist boat-like TS at the same C•••Si bond stretch.

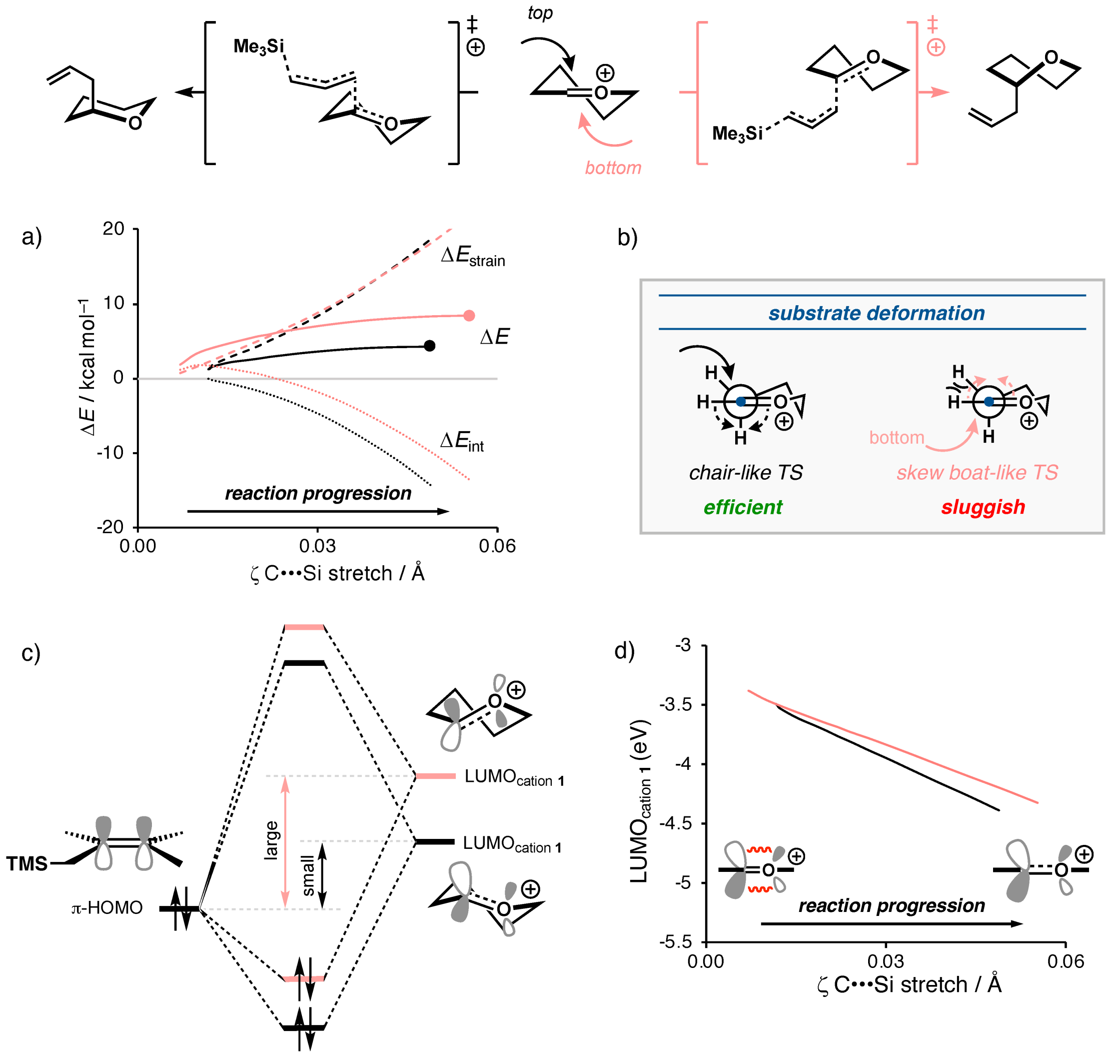

Figure 4. (a) Activation strain model and of the substrate for the S_E2' reactions of allyltrimethylsilane and cation **1** via the top face-attack (black: chair-like TS) and bottom face-attack (pink: twist boat-like TS), where the energy values are plotted to the transition state (indicated by a dot), along the IRC projected on the C•••Si bond stretch. (b) Schematic summary of the controlling factor of the facial selectivity of the oxocarbenium ion half chair conformation. (c) MO diagram of the most important donor–acceptor interaction between the π–$HOMO_{allyltrimethylsilane}$ and the $LUMO_{cation\ 1}$. (d) The LUMO energy ε (in eV) of the system described in the caption (a). Computed at COSMO(CH_2Cl_2)-ZORA-B3LYP/TZ2P//PCM(CH_2Cl_2)-B3LYP/6-311G(d,p).

The pyramidalization is essential for the reaction progression as the C1-atom transforms from a trigonal planar (sp^2) geometry in the starting oxocarbenium ion into a tetrahedral (sp^3) geometry in the product.

The effect of this higher degree of pyramidalization on the reaction path preference can be well understood with our recently introduced concept of a reaction's "transition state acidity",[19] which states that a more acidic substrate, possessing a LUMO of lower energy, will interact more strongly with a Lewis base (*i.e.*, electron-rich species). The LUMO of the oxocarbenium has mainly antibonding character in the C1=O$^+$ bond (red wiggle in Figure 4d). The elongation of the C–O bond along the reaction coordinate reduces this antibonding overlap, which leads to a stabilization of the LUMO orbital energy. The chair-like TS has a higher degree of pyramidalization than the twist boat-like TS, which results in a longer C1=O$^+$ bond of the oxocarbenium ion (C–O bond length: 1.311 Å and 1.306 Å for the chair-like and twist boat-like TS, respectively, at 0.049 Å C•••Si stretch). This increased C1=O$^+$ bond length reduces the antibonding overlap between p_z atomic orbitals of the C- and O-atom of the oxocarbenium ion, leading to a lower energy LUMO (more stabilized LUMO, Figure 4d). The resulting smaller $\text{HOMO}_{\text{allyltrimethylsilane}}$–$\text{LUMO}_{\text{cation }\mathbf{1}}$ translates to a more stabilizing orbital interaction (Figure 4c; see Figure S4 and Table S7 for EDA data).

One could expect that the more efficient deformation of the half chair to chair-like TS would also lead to less destabilizing strain for this reaction pathway. However, the more advanced pyramidalization for the chair-like TS at the same point on the reaction profile (at the same C•••Si bond stretch) as for the skew boat-like TS leads to an overall comparable strain development for both reaction pathways (Figure 4a).

After investigating the facial selectivity of the non-substituted half chair oxocarbenium ion, we analyzed the factors that control the stereoselectivity of the substituted cyclic oxocarbenium ion **2**-**5** by means of the ASM (see Table S7 for the ASM/EDA data on consistent geometries of **2-5**). Note, that in the following sections, we will use the lowest energy conformer as reference energy in the activation strain diagrams (ASDs) for both reaction paths, because this is the most descriptive way to delineate the analysis of the trends in reactivity and allows a direct connection to the $\Delta\Delta G^{\ddagger}$ shown in Figure 2 and 3. Furthermore, we will solely focus on the pathways proceeding through a chair-like TS for both the $^3H_4$ (black line) and $^4H_3$ (red line) conformers, as the twist boat-like TSs are significantly higher in energy, and thus less relevant.

Figure 5a and 5b show the activation strain diagrams (ASDs) of the S_E2' reaction of allyltrimethylsilane with C3-OMe cation **3** and C4-OMe cation **4**, as these exhibit similar characteristics. For cation **3**, the top face-attack is the preferred pathway (black line), and the

ASM analysis reveals that this preference originates from a less destabilizing strain energy for this pathway. For cation **4**, the bottom face-attack on the $^4H_3$-ion is favored (red line), which, likewise, can be traced back to the less destabilizing strain energy for this reaction path. For both cation **3** and **4** the developing interaction energy for the top and bottom face pathways is similar, and hence, does not account for the found reactivity trend.

By decomposing the total strain energy term into the strain energy of the individual reactants, it was found that the differences in strain energy solely originate from the oxocarbenium ion component and that the strain energy of allyltrimethylsilane is very similar

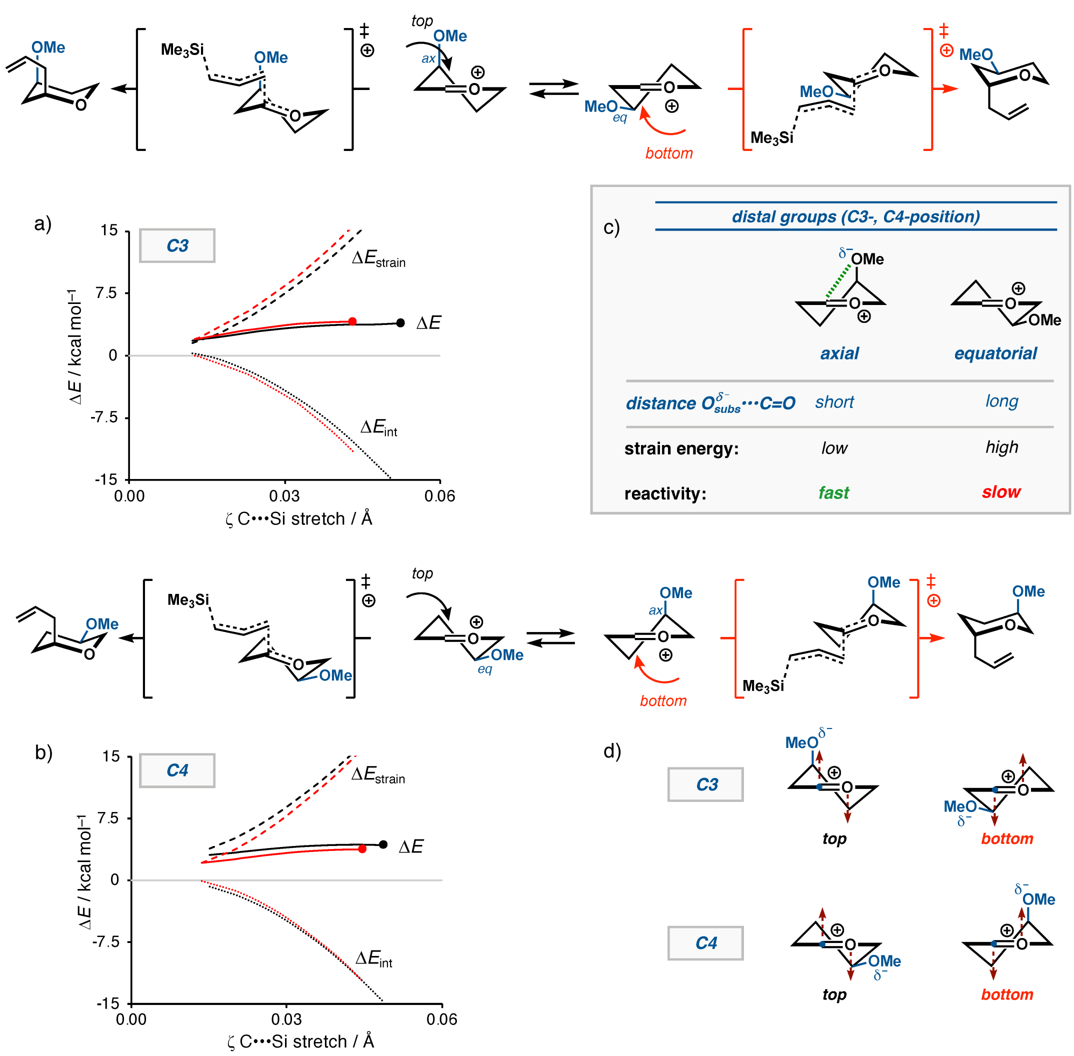

Figure 5. Activation strain model for the S_E2' reactions of allyltrimethylsilane + cation **3** (a) and **4** (b) via the top face-attack (black: chair-like TS) and bottom face-attack (red: chair-like TS), where the energy values are plotted to the transition state (indicated by a dot), along the IRC projected on the C•••Si bond stretch. (c) Schematic summary of the controlling factor of the stereoselectivity of the oxocarbenium ions with distal alkoxy substituents. (d) Movement of the C1=O$^+$ bond along the S_E2' reaction for cation **3** and **4**. Computed at COSMO(CH_2Cl_2)-ZORA-B3LYP/TZ2P//PCM(CH_2Cl_2)-B3LYP/6-311G(d,p).

for both reaction pathways (see Figure S6). The difference in strain of the oxocarbenium ions at the start of the reaction profile can be directly attributed to the conformational preference, *i.e.*, "intrinsic preference", of the oxocarbenium ion,[4a] with the $^3H_4$ conformer being most stable for cation **3** and the $^4H_3$-conformer being the most stable for ion **4**. Recall, that we used in our ASDs for both reaction paths the lowest energy conformer as reference energy. The addition to either face follows a similar reaction path through a chair-like transition state, providing strain curves with almost similar slopes, but the offset is significantly different as a result of the intrinsic stability of the conformation of the oxocarbenium ions (*i.e.*, "intrinsic preference"; Figure 5c).

Careful inspection of the strain curves reveals that the curves for cation **4** slightly converge along the reaction coordinate, while the curves for cation **3** slightly diverge. This explains why the "intrinsic preference" of the cation ($\Delta\Delta G^{o}$) does not directly correlate to the difference in the corresponding overall reaction barriers ($\Delta\Delta G^{\ddagger}$) for these reactions. The divergence and convergence of the strain curves of the reactions can be traced back to the deformation of both half chairs along the reaction coordinate. For cation **3**, the top face-attack at the $^3H_4$ conformer brings the C1-atom closer to the stabilizing axial C3-OMe group (black path; Figure 5d), while this is not the case for the $^4H_3$ conformer (red path; see Figure S7 for more information), diverging the strain curves along the reaction coordinate. For cation **4**, the electrophilic anomeric C1-atom is pulled away from the stabilizing axial C4-OMe group in going from the $^4H_3$ conformer to the chair-like TS (red path), resulting in increased destabilization of the cation. This effect is significantly less for the reaction taking place with the $^3H_4$ conformer (black path), and as a result, the two strain curves converge along the reaction coordinate.

Next, we turned to the ASDs of the S_E2' reaction of allyltrimethylsilane with the oxocarbenium ions bearing the substituent closer to the C-1 atom, the C5-CH_2OMe cation **5** and the C2-OMe cation **2**. Oxocarbenium ion **5** preferentially undergoes a bottom face-attack, which, in line with the S_E2' reactions of cation **3** and **4**, can be traced back to the less destabilizing strain developing in this reaction pathway. However, the difference in strain energy between the top and bottom face reaction around the start of the reaction ($\Delta\Delta E \sim -2$ kcal mol^{-1} for the $^4H_3$ relative to the $^3H_4$ conformer) is significantly larger than the intrinsic energy difference between the $^3H_4$ and $^4H_3$ conformers ("intrinsic preference") of cation **5** (see Figure 3). By analyzing the reaction path for the top face-attack, which takes place on the $^3H_4$-cation, it becomes clear that allyltrimethylsilane comes in close proximity to the *pseudo*-axial C5-CH_2OMe-substituent, resulting in steric repulsion between the two reactants.

10.1002/chem.202203490

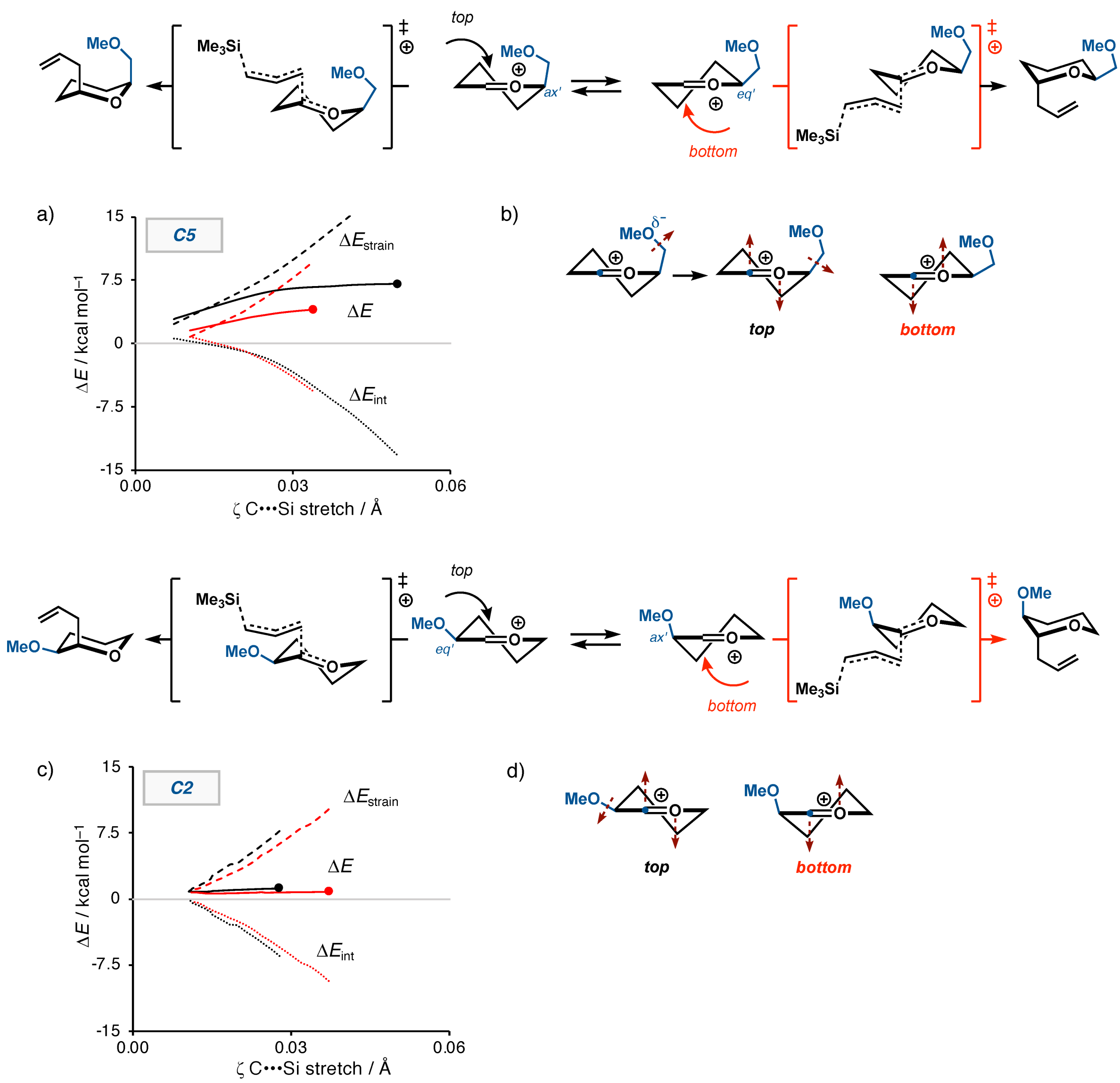

Figure 6. (a,c) Activation strain model for the S_E2' reactions of allyltrimethylsilane + cation **5** and **2** via the top face-attack (black: chair-like TS) and bottom face-attack (red: chair-like TS), where the energy values are plotted to either the transition state or a local maximum (indicated by a dot), along the IRC projected on the C•••Si bond stretch. (b,d) Movement of the C1=O$^+$ bond and substituent along the S_E2' reaction for cation **5** and **2**. Computed at COSMO(CH_2Cl_2)-ZORA-B3LYP/TZ2P//PCM(CH_2Cl_2)-B3LYP/6-311G(d,p).

This steric repulsion can be minimized by bending the substituent away. Consequently, this leads to more destabilizing strain energy due to the deformation of the reactant along the complete reaction profile (see Figure S7c). Note that steric repulsion between the reactants can manifest in both: (i) the strain energy, because steric repulsion deforms the fragments, and (ii) the steric (Pauli) repulsion found in the nucleophile–electrophile interaction.[20] In this case the steric repulsion is primarily absorbed into the strain term, leading to additional deformation of the cation. The steric repulsion between the C5-CH_2OMe-substituent and allyltrimethylsilane renders cation **5** substantially more bottom face selective than what would be expected based on the intrinsic preference of the cation. Intuitively, one could expect a similar scenario for cation **3**, in which the axial C-3 substituent can also engage in steric interactions with the incoming allyltrimethylsilane. However, the C-3 OMe-substituent is significantly smaller than the C-5 CH_2OMe substituent, avoiding excessive steric repulsion.[21]

Analogous to the strain curves for cation **4**, the strain curves for cation **5** slightly converge along the reaction coordinate. Again, this stems from the deformation of both half chairs as the reaction progresses. For the transformation of the $^4H_3$ conformation to the chair-like TS (red path), the electrophilic anomeric C1-atom is pulled away from the stabilizing *pseudo*-axial C5-CH_2OMe group resulting in the overall destabilization of the cation (Figure 6b). This effect is less apparent for the reaction taking place on the $^3H_4$ conformer (black path).

Finally, the ASD of the reactions on the C2-OMe cation **2** shows that there is only a marginal difference in the transition state energies of the top- and bottom face reactions. The similar strain energy of the oxocarbenium ions at the start of the reaction profile is related to the similar energy of the $^3H_4$ and $^4H_3$-conformers (+0.1 kcal mol^{-1} for the $^4H_3$ relative to the $^3H_4$). The strain curves diverge upon the progression of the reaction coordinate, which can be explained by the 2-OMe bending away from the allylic moiety, which comes in from the same side, to minimize steric interactions. The bottom face approach avoids this steric interaction, resulting in a slightly lower reaction barrier for the bottom-face reaction (red pathway; $\Delta\Delta G^{\ddagger}$ = –0.2 kcal mol^{-1} for the $^4H_3$ relative to the $^3H_4$).

Conclusions

Our computational investigation has revealed that S_E2' reactions of allyltrimethylsilane with six-membered oxocarbenium ions can follow reaction pathways proceeding with a chair-like and twist boat-like transition state. For all studied cases, the chair-like TS has a significantly lower reaction barrier than the twist boat-like TS. Our activation strain and Kohn-Sham molecular orbital theory analyses reveal that the facial preference for the chair-like TS, compared to the skew boat-like TS, originates from a more efficient geometric deformation (pyramidalization of C1) in transitioning from the half chair starting compound to the chair-like TS.

The introduction of alkoxy substituents on the six-membered oxocarbenium ion strongly impacts the stereochemical outcome and reactivity of the studied S_E2' reactions. Overall, the reaction barriers decreased by placing the alkoxy substituent systematically closer to the electrophilic C1-position. This is a direct effect of the electron-withdrawing effect of the substituent, which stepwise increases the electron-accepting capability of the C1-atom of the oxocarbenium ion. Moreover, the activation strain analyses showed that the stereoselectivity of the addition reactions of allyltrimethylsilane to the oxocarbenium ions is primarily set by the energy difference between the half chair conformers (*i.e.* the "intrinsic preference" of the cations) as the most stable oxocarbenium ion conformers led to the lowest-energy reaction barrier. Strikingly, for the C5-CH_2OMe-substituted cation, it was found that steric interactions between the relatively large C5-substituent and allyltrimethylsilane developed, resulting in a significantly more *trans*-selective reaction for the C5-CH_2OMe cation, than what would be expected based on the relative energy of the two half chair oxocarbenium ions.

Overall, this study has dissected the effects at play during the addition of a typical *C*-nucleophile to mono-substituted six-membered oxocarbenium ions. The fundamental mechanistic insight provided in this contribution will be helpful in understanding the reactivity of more complex glycosyl cations featuring multiple substituents and will aid in the general understanding of glycosylation reactions.

ORCID

Wouter A. Remmerswaal: 0000-0002-1040-4311
Thomas Hansen: 0000-0002-6291-1569
Trevor A. Hamlin: 0000-0002-5128-1004
Jeroen D. C. Codée: 0000-0003-3531-2138

Supporting Information

Computational methods, Additional computational results; Cartesian coordinates, energies, and the number of imaginary frequencies of all stationary points.

Acknowledgments

Quantum chemical calculations were performed at the SURFsara HPC center in Amsterdam (2021/ENW/01070753 awarded to J.D.C.C). This work was supported by an ERC-CoG (726072) and NWO VICI (VI.C.182.020) grant awarded to J.D.C.C.

Competing interest

The authors declare no competing interests.

Table of contents

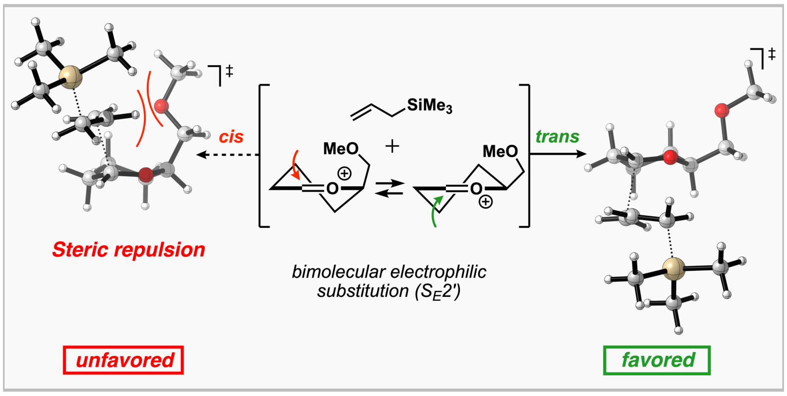

Bottoms up! Quantum chemical analyses of the transition states of S_E2' reactions between substituted six-membered oxocarbenium ions and allyltrimethylsilane have provided quantitative insight into the stereoelectronic effects of the ring substituents, which dictate the stereoselectivity of the additions.

References and notes

[1] (a) P. Merino, I. Delso, S. Pereira, S. Orta, M. Pedrón, T. Tejero, *Org. Biomol. Chem.*, **2021**, *19*, 2350–2365. (b) L. Bohé, D. Crich, *Carbohydr. Res.* **2015**, *403*, 48–59. (c) M. T. C. Walvoort, J. Dinkelaar, L. J. van den Bos, G. Lodder, H. S. Overkleeft, J. D. C. Codée, G. A. van der Marel, *Carbohydr. Res.* **2010**, *345*, 1252–1263. (d) D. Crich, *Acc. Chem. Res.* **2010**, *43*, 1144–1153. (e) P. O. Adero, H. Amarasekara, P. Wen, L. Bohé, D. Crich, *Chem. Rev.* **2018**, *118*, 8242–8284. (f) L. K. Mydock, A. V. Demchenko, *Org. Biomol. Chem.* **2010**, *8*, 497–510. (g) M. T. Yang, K. A. Woerpel, *J. Org. Chem.* **2009**, *74*, 545–553.

[2] A. Ardèvol, C. Rovira, *Angew. Chem. Int. Ed.* **2011**, *50*, 10897–10901; *Angew. Chem.* **2011**, *123*, 11089–11093. (b) M. A. Morais, J. Coines, M. N. Domingues, R. A. Pirolla, C. C. Tonoli, C. R. Santos, J. B. L. Correa, F. C. Gozzo, C. Rovira, M. T. Murakami, *Nat. Commun.* **2021**, *12*, 1–13.

[3] (a) C. W. Chang, M. H. Lin, C. C. Wang, *Chem. Eur. J.* **2021**, *27*, 2556–2568. (b) A. V. Demchenko, Handbook of Chemical Glycosylation: Advances in Stereoselectivity and Therapeutic Relevance, Wiley, **2008**. (c) S. S. Nigudkar, A. V. Demchenko, *Chem. Sci.* **2015**, *6*, 2687–2704. (d) C. -H. Hsu, S. -C. Hung, C. -Y. Wu, C. -H. Wong, *Angew. Chem. Int. Ed.* **2011**, *50*, 11872–11923. (e) C. W. Chang, M. H. Lin, C. H. Wu, T. Y. Chiang, C. C. Wang, *J. Org. Chem.*, **2020**, *85*, 15945–15963. (f) J. -C. Lee, W. A. Greenberg, C. -H. Wong, *Nat. Protocols* **2007**, *1*, 3143–3152. (g) J. Chen, T. Hansen,

Q. -J, Zhang, D. -Y. Liu, Y. Sun, H. Yan, J. D. C. Codée, R. R. Schmidt, J. -S. Sun, *Angew. Chem. Int. Ed.* **2019**, *58*, 17000–17008; *Angew. Chem.* **2019**, *131*, 17156–17164. (h) S. van der Vorm, T. Hansen, J. M. van Hengst, H. S. Overkleeft, G. A. van der Marel, J. D. C. Codée, *Chem. Soc. Rev.* **2019**, *48*, 4688–4706.

[4] (a) K. M. Demkiw, W. A. Remmerswaal, T. Hansen, G. A van der Marel, J. D. C. Codée, K. A. Woerpel, *Angew. Chem. Int. Ed.* **2022**, e202209401; *Angew. Chem.* **2022**, e202209401 (b) T. Hansen, L. Lebedel, W. A. Remmerswaal, S. van der Vorm, D. P. A. Wander, M. Somers, H. S. Overkleeft, D. V. Filippov, J. Désiré, A. Mingot, Y. Bleriot, G. A. van der Marel, S. Thibaudeau, J. D. C. Codée, *ACS Cent. Sci.* **2019**, *5*, 781–788. (c) S. van der Vorm, T. Hansen, E. R. van Rijssel, R. Dekkers, J. M. Madern, H. S. Overkleeft, D. V. Filippov, G. A. van der Marel, J. D. C. Codée, *Chem. Eur. J.* **2019**, *25*, 7149–7157. (d) S. van der Vorm, T. Hansen, E. R. van Rijssel, R. Dekkers, J. M. Madern, H. S. Overkleeft, D. V. Filippov, G. A. van der Marel, J. D. C. Codée, *Chem. Eur. J.* **2019**, *25*, 7149–7157. (e) T. Hansen, T. P. Ofman, J. G. C. Vlaming, I. A. Gagarinov, J. van Beek, T. A. Goté, J. M. Tichem, G. Ruijgrok, H. S. Overkleeft, D. V. Filippov, G. A. van der Marel, J. D. C. Codée, *Angew. Chem. Int. Ed.* **2021**, *60*, 937–945; *Angew. Chem.* **2021**, *133*, 950–958. (f) E. R. van Rijssel, P. van Delft, G. Lodder, H. S. Overkleeft, G. A. van der Marel, D. V. Filippov, J. D. C. Codée, *Angew. Chem. Int. Ed.*, **2014**, *53*, 10381–10385; *Angew. Chem.* **2014**, *126*, 10549–10553.

[5] (a) A. Martin, A. Arda, J. Désiré, A. Martin-Mingot, N. Probst, P. Sinaÿ, J. Jiménez-Barbero, S. Thibaudeau, Y. Blériot, *Nat. Chem.* **2016**, *8*, 186–191. (b) H. Elferink, M.E. Severijnen, J. Martens, R. A. Mensink, G. Berden, J. Oomens, F. P. J. T. Rutjes, A. M. Rijs, T. J. Boltje, *J. Am. Chem. Soc.* **2018**, *140*, 6034–6038. (c) T. Hansen, H. Elferink, J. M. A. van Hengst, K. J. Houthuijs, W. A. Remmerswaal, A. Kromm, G. Berden, S. van der Vorm, A. M. Rijs, H. S. Overkleeft, D. V. Filippov, F. P. J. T. Rutjes, G. A. van der Marel, J. Martens, J. Oomens, J. D. C. Codée, T. J. Boltje, *Nat. Commun.* **2020**, *11*, 2664. (d) K. Saito, K. Ueoka, K. Matsumoto, S. Suga, T. Nokami, J. Yoshida, *Angew. Chem. Int. Ed.* **2011**, *50*, 5153–5156; *Angew. Chem.* **2011**, *123*, 5259–5262. (e) L. Lebedel, A. Ardá, A. Martin, J. Désiré, A. Mingot, M. Aufiero, N. Aiguabella, R. Gilmour, J. Jiménez-Barbero, Y. Blériot, S. Thibaudeau, *Angew. Chem. Int. Ed.* **2019**, *58*, 13758–13762; *Angew. Chem.* **2019**, *131*, 13896–13900. (f) H. Elferink, R. A. Mensink, W. W. A. Castelijns, O. Jansen, J. P. J. Bruekers, J. Martens, J. Oomens, A. M. Rijs, T. J. Boltje, *Angew. Chem. Int. Ed.* **2019**, *58*, 8746–8751; *Angew. Chem.* **2019**, *131*, 8838–8843. (g) M. Marianski, E. Mucha, K. Greis, S. Moon, A. Pardo, C.

10.1002/chem.202203490

Kirschbaum, D. A. Thomas, G. Meijer, G. von Helden, K. Gilmore, P. H. Seeberger, K. Pagel, *Angew. Chem. Int. Ed.* **2020**, *59*, 6166–6171. (h) E. Mucha, M. Marianski, F. -F. Xu, D. A. Thomas, G. Meijer, G. von Helden, P. H. Seeberger, K. Pagel, *Nat. Commun.* **2018**, *9*, 4174. (i) W. A. Remmerswaal, K. J. Houthuijs, R. van de Ven, H. Elferink, T. Hansen, G. Berden, H. S. Overkleeft, G. A. van der Marel, F. P. J. T. Rutjes, D. V. Filippov, T. J. Boltje, J. Martens, J. Oomens, J. D. C. Codée, *J. Org. Chem.* **2022**, *87*, 9139–9147. (j) H. Elferink, W. A. Remmerswaal, K. J. Houthuijs, O. Jansen, T. Hansen, A. M. Rijs, G. Berden, J. Martens, J. Oomens, J. D. C. Codée, T. J. Boltje, *Chem.Eur. J.* **2022**, e202201.

[6] (a) T. Hosoya, T. Takano, P. Kosma, T. Rosenau, *J. Org. Chem.* **2014**, *79*, 7889–7894. (b) T. Hosoya, P. Kosma, T. Rosenau, *Carbohydr. Res.* **2015**, *401*, 127–131. (c) M. Huang, G. E. Garrett, N. Birlirakis, L. Bohé, D. A. Pratt, D. Crich, *Nat Chem* **2012**, *4*, 663–667. (d) T. Nukada, A. Bérces, L. Wang, M. Z. Zgierski, D. M. Whitfield, *Carbohydr. Res.* **2005**, *340*, 841−852. (e) T. Hansen, P. Vermeeren, F. M. Bickelhaupt, T. A. Hamlin, *Chem. Commun.* **2022**, *58,* 12050–12053.

[7] (a) L. Ayala, C. G. Lucero, J. A. C. Romero, S. A. Tabacco, K. A. Woerpel, *J. Am. Chem. Soc.* **2003**, *125*, 15521–15528. (b) C. G. Lucero, K. A. Woerpel, *J. Org. Chem.* **2006**, *71*, 2641–2647.

[8] P. Deslongchamps, Y. L. Dory, S. Li, *Can. J. Chem.* **1994**, *10*, 2021–2027.

[9] R. V. Stevens, A. W. M. Lee, *J. Am. Chem. Soc.* **1979**, *101*, 7032–7035. (b) P. Deslongchamps, Stereoelectronic Effects in Organic Chemistry, Pergamon: New York, **1983**, pp 209–221.

[10] (a) S. Chamberland, J. W. Ziller, K. A. Woerpel, *J. Am. Chem. Soc.* **2005**, *127*, 5322–5323. (b) J. A. C. Romero, S. A. Tabacco, K. A. Woerpel, *J. Am. Chem. Soc.* **2000**, *122*, 168–169. (c) S. van der Vorm, T. Hansen, H. S. Overkleeft, G. A. van der Marel, J. D. C. Codée, *Chem. Sci.* **2017**, *8*, 1867–1875. (d) J. -F. Parent, G. Deslongchamps, P. Deslongchamps, *J. Org. Chem.* **2020**, *85*, 4220–4236.

[11] Me_3Si^+ eventually reacts with a TfO^- to form Me_3SiOTf in the final product (P in Table S1, S2 and S3). All stationary points, except the product, includes the energy of a single TfO^- molecule.

[12] In recent years, domain based local pair natural orbitals (DLPNO) have been used to significantly lower the computational cost, while maintaining chemical accuracy, of coupled cluster theory with single-, double-, and perturbative triple excitations (CCSD(T)).

[13] (a) M. J. Buckle, I. Fleming, S. Gil, K. L. C. Pang, *Org. Biomol. Chem.* **2004**, *2*, 749–769. (b) M. J. Buckle, I. Fleming, S. Gil, *Tetrahedron Lett.* **1992,** *33*, 4479–4482. (c) I. Fleming, K. L. C. Pang, *Tetrahedron Lett.* **2002**, *43*, 5985–5988. (d) E. Casali, A. Porta, L. Toma, G. Zanoni, *J. Org. Chem.* **2022**, *87*, 9497−9506.

[14] (a) P. Vermeeren, S. C. C. van der Lubbe, C. Fonseca Guerra, F. M. Bickelhaupt, T. A. Hamlin, *Nat. Protoc.* **2020**, *15*, 649–667. (b) F. M. Bickelhaupt, K. N. Houk, *Angew. Chem., Int. Ed.* **2017**, *56*, 10070–10086; *Angew. Chem.* **2009**, *129*, 10204–10221.

[15] (a) F. M. Bickelhaupt, E. J. Baerends, Kohn-Sham Density Functional Theory: Predicting and Understanding Chemistry. In *Reviews in Computational Chemistry*, K. B. Lipkowitz, D. B. Boyd, Eds., Wiley-VCH: New York, **2000**, Vol. *15*, pp 1–86. (b) R. van Meer, O. V. Gritsenko, E. J. Baerends, E. J. *J. Chem. Theory Comput.* **2014**, *10*, 4432–4441.

[16] The dispersion-corrected PCM(CH_2Cl_2)-B3LYP-D3(BJ)/6-311G(d,p) approach rendered proivides reactivity trends compared to PCM(CH_2Cl_2)-B3LYP/6-311G(d,p) (Table S3 and S6).

[17] (a) J. I. Seeman, *J. Chem. Educ.* **1986**, *63*, 42. (b) J. I. Seeman, *Chem. Rev.* **1983**, *83*, 83–134.

[18] Q. Peng, F. Duarte, R. S. Paton, *Chem. Soc. Rev.* **2016**, *45*, 6093–6107.

[19] (a) P. Vermeeren, T. Hansen, P. Jansen, M. Swart, T. A. Hamlin, and F. M. Bickelhaupt, *Chem. Eur. J.* **2020**, *26*, 15538–15548. (b) P. Vermeeren, T. Hansen, M. Grasser, D. Rodrigues Silva, T. A. Hamlin and F. M. Bickelhaupt, *J. Org. Chem*. **2020**, *85*, 14087; (c) T. Hansen, J. C. Roozee, F. M. Bickelhaupt and T. A. Hamlin, *J. Org. Chem.* **2022**, *87*, 1805. (d) T. Hansen, P. Vermeeren, F. M. Bickelhaupt, and T. A. Hamlin, *Angew. Chem. Int. Ed.* **2021**, *60*, 20840–20848; *Angew. Chem.* **2021**, *133*, 21008–21016. (e) T. Hansen, P. Vermeeren, L. de Jong, F. M. Bickelhaupt, T. A. Hamlin, *J. Org. Chem*. **2022**, *87*, 8892–8901. (f) T. Hansen, A. Nin-Hill, J. D. C. Codée, T. A. Hamlin, C. Rovira, *Chem. Eur. J.* **2022**, *28*, e202201649.

[20] T. Hansen, X. Sun, M. Dalla Tiezza, W. -J. van Zeist, J. N. P. van Stralen, D. P. Geerke, L. P. Wolters, T. A. Hamlin, F. M. Bickelhaupt, *Chem. Eur. J.* **2022**, *28*, e202201093

[21] Installing an OMe-substituent at the C5-position, instead of the C5-CH_2OMe-substituent, results in more similar behavior as found for cation **3** and **4** (see SI Figure S1, S2 and SI Table S1 and S2 for data), in which the difference in strain of the oxocarbenium ions at the start of the reaction profile can be directly attributed to the conformational preference of the cation.